The Bioscan
AN INTERNATIONAL QUARTERLY JOURNAL OF LIFE SCIENCES
21(1): 685-731, 2026 www.thebioscan.com

Advanced growth and multifunctional characterization of L-Threonine single crystals: comprehensive Insights from structural, Functional, Optical, Mechanical, Antibacterial and Thermal properties with potential in optoelectronics, photonics and Nonlinear optical applications.

N. Rajasekar[1], K. Balasubramanian[2*]
[1]Research scholar (Reg.No: 22211072131006), PG and Research department of physics, The M.D.T Hindu college, Pettai, Tirunelveli-627010, Tamilnadu, India.
[2]Associate professor, PG and Research department of physics, The M.D.T Hindu college, Pettai, Tirunelveli-627010, Tamilnadu, India.
[1,2]Affillated by Manonmaniam Sundarnar University, Abishekapatti-627012, Tirunelveli, Tamilnadu, India.

Corresponding author: K. Balasubramanian, E-mail: rs9012618@gmail.com

DOI: 10.63001/tbs.2026.v21.i01.pp685-731

Keywords
W-H Plot, Functional, Morphological, Mechanical, Thermal parameters: Broidos and Kissinger methods, Antibacterial: E. coli and S. Aureus, Opto-electronics, Photonics and nonlinear optics.

Received on:

25-11-2025

Accepted on:

18-12-2025

Published on:

29-01-2026

ABSTRACT

High-quality Single crystals of an organic nonlinear optical (NLO) material were obtained at room conditions via the slow solvent evaporation technique. The crystalline structure and phase purity were established through PXRD studies. Fourier transform infrared (FTIR) spectroscopy was utilized to investigate the presence of characteristic functional groups and molecular interactions. In addition to optical transparency (%) and direct bandgap evaluation via UV-Vis spectroscopy, the refractive index, reflectance, optical conductivity, and extinction coefficient were analyzed to provide a comprehensive insight into the material's optical characteristics. Morphological surface features were examined through scanning electron microscopy (SEM). The EDX spectra revealed the presence of constituent elements with a uniform distribution and no detectable impurities, indicating the chemical purity and compositional homogeneity of the material. Third harmonic generation in L-Threonine crystalline samples was studied using the Z-scan technique. The photoluminescence emission peak at 466 nm was observed, corresponding to a electronic transition of 2.66 eV. CHN analysis verified the elemental constituents of the material, revealing the expected percentages of carbon, hydrogen, and nitrogen, thereby indicating its chemical purity and stoichiometric consistency. Thermal properties associated with the sample was evaluated through differential thermal analysis (DTA) and derivative thermogravimetry (DTG), where the theromogravimetric (TG) was determined, and the kinetic parameters of decomposition were evaluated employing both the kissinger and broidos method. Antibacterial studies against S. aureus and E. Coli revealed no inhibitory activity, indicating that the material is inactive as a bioactive agent. 1H and 13C FT NMR analyses of the material confirmed the characteristic chemical shifts of α and β-Protons, methyl protons, carboxyl carbon, and hydroxyl-bearing carbon, consistent with its amino acid structure. The comprehensive results possesses favorable optical, thermal and mechanical properties, rendering it a suitable material for photonic, optoelectronic and Nonlinear-optical applications.

Introduction

L-Threonine, is among the 20 amino acids involved in human metabolism and is classified as an indispensible amino acid, necessary for proteins biosynthesis, playing a vital role in various metabolic functions. It is widely used in Medical Laboratories and various industries. L-Threonine is the simpliest and essential amino acids is particularly well-suited for crystal growth research because of its optical transparency, Good solubility in water, hydrogen-bonding ability, and zwitterionic nature **[1, 2]**. These attributes establish it as an efficient organic crystals for nonlinear optical (NLO) applications **[3]**. L-Threonine has both amino ($–NH_2$) and carboxyl (–COOH) functional groups, in combination with the hydroxyl (-OH) moiety in its side chain. These groups enable strong intermolecular hydrogen bonding, which helps stabilize the crystal lattice. Its natural chirality and zwitterionic nature enhance optical transparency and mechanical stability, which are fundamental prerequisites for third harmonic generation (THG) and other third-order Nonlinear optical processes **[4]**. L-Threonine crystallizes in a non-centrosymmetric orthorhombic system, an essential requirement for second-order nonlinear optical processes and related optical phenomena **[5]**.

Applications

In recent years, L-Threonine single crystals have garnered considerable attention owing to their promising Nonlinear optical (NLO) applications in photonics and optoelectronic devices. The single crystals have attracted attention for photonics, optoelectronics, and nonlinear optical applications, attributed to their superior optical transparancy and mechanical characteristics. These crystal possess a wide band gap, good optical transparency, and favorable photoluminescence properties, making them suitable for optical switches, sensors, and frequency conversion devices. In addition, their mechanical stability and

chemical purity enhance their potential for practical applications. This work aims focuses on investigate the growth and comprehensive detailed properties of L-Threonine sample to evaluate the structural, optical, mechanical and functional properties using Powder-XRD, Fourier transform infrared spectroscopy, Ultraviolent-visible analysis, scanning electron microscopy, Energy dispersive X-ray, Elemental analysis, TG/DTA, antibacterial studies, Z-scan, photoluminescence, 1H FT NMR and 13C FT NMR and microhardness measurements **[6-7]**.

Material synthesis

Analytical-grade L-Threonine was utilized as the starting material for crystal growth experiment. An accurately weighed quantity of 5 grams of L-Threonine was solubilized using deionized water under ambient conditions. The precursor solution was maintained under continuous stirring for 5 hrs with a magnetic stirrer in order to acheive complete dissolution and to acheive homogeneity. After stirring, the solution was subjected to filtration through whatmann filter paper to remove insoluable contaminants. The obtained filterate was transferred into the clean crystallization vessel and left undisturbed under ambient condition. Over a span of 15 days, controlled solvent evaporation resulted in nucleation, leading to formation of well-defined L-Threonine crystals. This method allows transparent, well-faceted single crystals to form.

The molecular formula of L-Threonine is $C_4H_9NO_3$

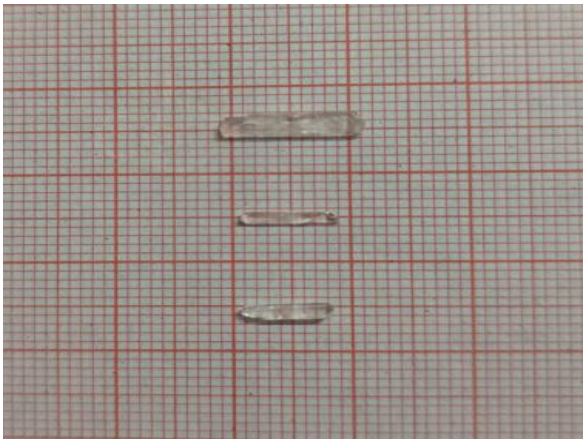

Fig : 1 Photographic image of L-Threonine single crystals

Results and Discussion

1). Powder X-ray diffraction analysis

The P-XRD characterization confirmed that the synthesized L-Threonine material adopted an orthorhombic structure belonging to the $P2_12_12_1$, space group, as evidenced by the sharp and well-resolved diffraction peaks. The lattice parameters a = 7.738 A°, b = 13.62 A°, c = 5.137 A°, axial angles $\alpha = \beta = \gamma = 90°$ and unit cell volume V = 541.60, were determined from the P-XRD technique, confirming the structural system of L-Threonine. Thus, the observed peaks are indexed with corresponding (13.010), (17.471), (18.495), (20.726), (21.727), (23.138), (26.188), (28.624), (29.625), (31.855), (35.110), (37.341), (39.366), (42.189), (45.238) values, and the most intense diffraction peak appeared along the (110), (120), (011), (101), (111), (200), (031), (131), (211), (221), (240), (022), (311), (132), (161) plane, which signifies the preferred orientation and high degree of crystallinity of the sample **[8]**. Figure (2) depicts the XRD graph of the sample, with peaks corresponding to its crystalline planes.

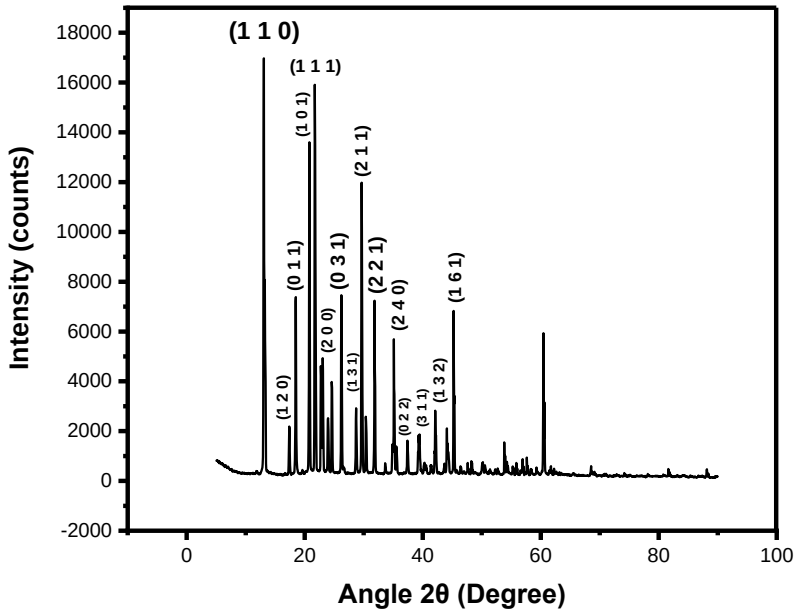

Fig. 2: X-ray diffraction profile of the grown crystal

The Hall-Williamson technique were employed for P-XRD patterns for the assessment of microstructural characteristics of the material. This method enabled the simultaneous evaluation of crystallite size and lattice strain by considering both the peak and broadening due to finite crystallite dimensions and strain-induced broadening. The Williamson-Hall analysis provided quantitative insight into the crystal lattice imperfections, including dislocation density and microstrain, thereby offering a detailed insight into material's structural integrity and defect distribution.

Thus, the Crystalline size (nm), dislocation density (δ), and microstrain (η) of the sample was evaluated using a powder XRD Williamson-Hall method. The analysis yielded a crystallite size of 31.95 nm, a dislocation density of 9.80 x 10^{-4} nm^{-2}, and a microstrain of 3.55 x 10^{-4}, with the willaimson-Hall showing a slope of -0.00142 and an intercept of 0.00434, indicating uniform strain distribution within the crystal lattice **[9]**.

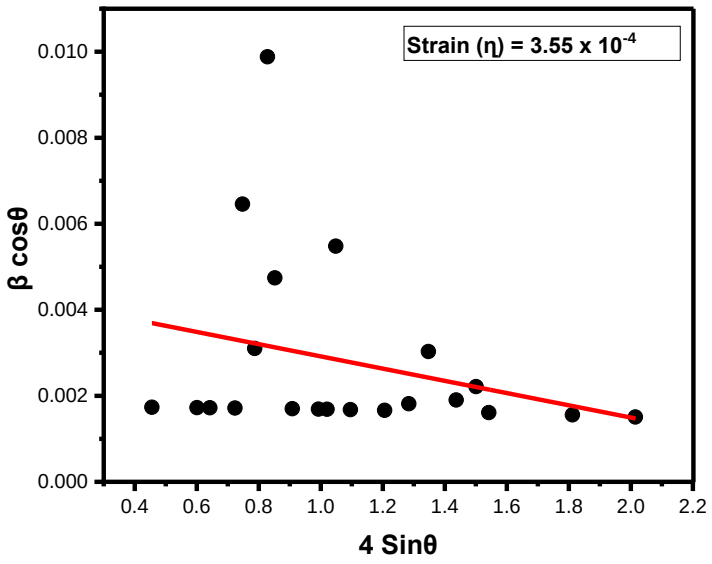

Fig. 3 Hall willaimson plot of L-Threonine

Table.1

Structural parameters	**values**
Maximum peak (2θ)	13.010
FWHM (β)	0.004340 radians
Crystallite size	31.95 nm
Dislocation density (δ)	9.80 x10-4 nm^{-2}
Microstrain (η)	3.55 x 10^{-4}
Slope	-0.00142
Intercept	0.00434

Degree of crystallinity	82.8 %

---

2). FTIR analysis

FTIR studies were carried out the spectral region of 400-4000 cm^{-1} to identify the moieties/Alcohol groups confirmed within the sample **[10]**. The first prominent peak is located at 413.47 cm^{-1}. A prominent absorption band appeared at 442.20 cm^{-1}. A distinct absorption band appears at 489.39 cm^{-1}.A characteristic band recorded at 767.44 cm^{-1}. A characteristic band appears at 873.11 cm^{-1}. The FTIR band is found at 930.57 cm^{-1}. A strong band is appeared around 1035.22 cm^{-1}. A characteristic FTIR band appears at 1102.94 cm^{-1}. A prominent vibrational band is evident at 1189.12 cm^{-1}. The FTIR band is observed at 1246.58 cm^{-1}. The spectrum displays an absorption band at 1341.99 cm^{-1}. The absorption feature appeared 1418.94 cm^{-1}. A prominent absorption band is evident at 1447.67 cm^{-1} .The spectrum shows a characteristic vibrational mode at 1620.04 cm^{-1}. A band obtained around 2874.82 cm^{-1}. A distinct vibrational band is detected at 2970.24 cm^{-1}. A characteristic absorption feature appears around 3171.34 cm^{-1}. Fig (3) displays the FTIR graph of the sample, indicating its characteristic absorption bands **[11, 12].**

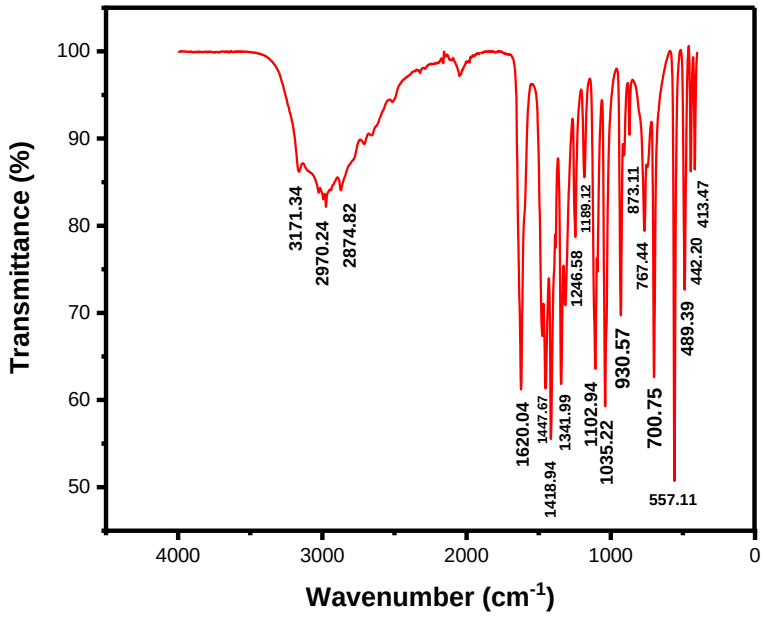

Fig. (3): FTIR spectrum depicts functional groups peaks

3). Uv-visible Liquid analysis

UV-vis analysis for the L-Threonine solution dissolved in distilled solvent were performed from 200-800 nm to study its optical properties and electronic transitions **[13, 14]**. The spectrum low absorbance across the full visible region and exhibited a absorption edge appearing at 247 nm attributed with an electronic excitation, likely of the (n-π*) type, indicating a wide band gap. The wide optical transparency window along with the observed cutoff at 230 nm associated with an electronic excitation in the (n-π*) type, demonstrates the material's potential for optoelectronic and nonlinear optical devices. The UV-Vis spectrum revealed a maximum transmittance of 90 %, indicating excellent light transmission in the visible spectrum.

Ultraviolent visible spectral analysis revealed that the sample shows excellent optical transmission across the visible range, with a well-defined cutoff, confirming its potential for photonic applications.

The UV-vis graph displayed minimal absorption within the visible range and a distinct absorption onset, which reflects the excellent optical properties and suitable of the material for nonlinear optical studies.

The Transmission profile obtained from UV-vis spectroscopy demonstrated a broad transparency window, and the identified cut-off wavelength lies in the near UV region, a characteristic feature desirable for frequency conversion devices

UV-vis spectral analysis revealed a energy band gap and reduced absorption losses of the sample, thereby ensuring its applicability in optoelectronic applications **[15]**.

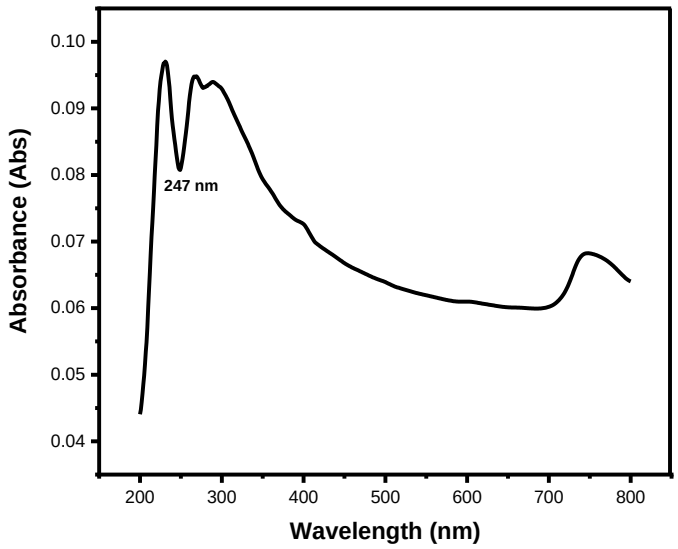

Fig.3 (a) UV-vis absorbance

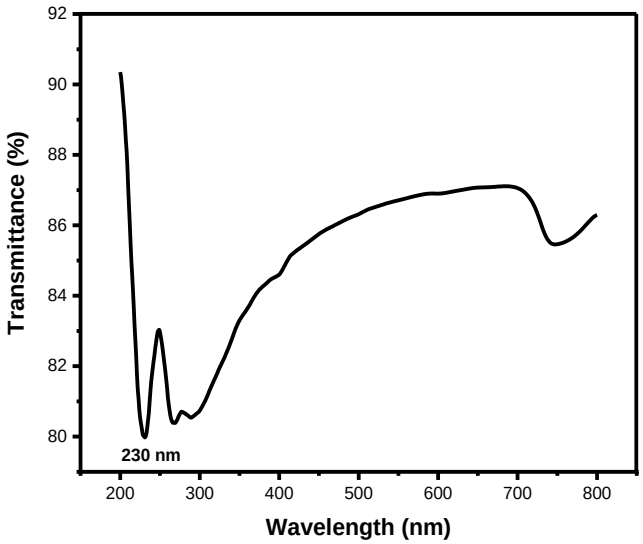

Fig.3 (b) UV-vis transmittance

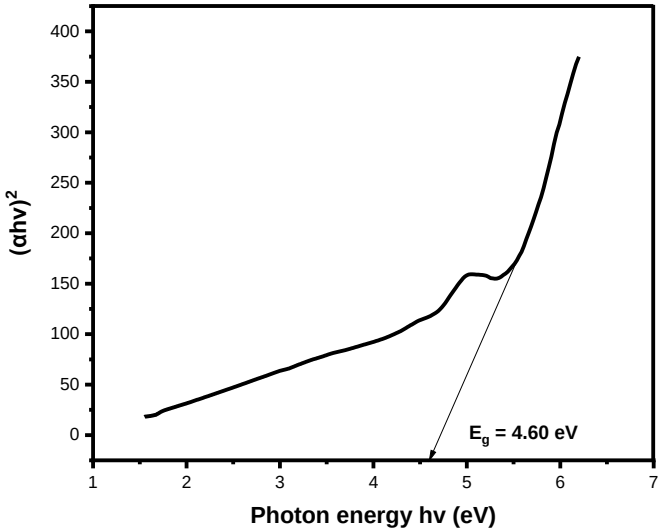

Fig.3 (c) UV-vis direct band gap

The Tauc plot of direct bandgap of the sample was determined by employing the Tauc method, using, $(\alpha hv)^2$ is plotted against the photon energy (hv) in the UV-vis range, and the linear region from the resulting plot is extrapolated to estimate the energy bandgap.

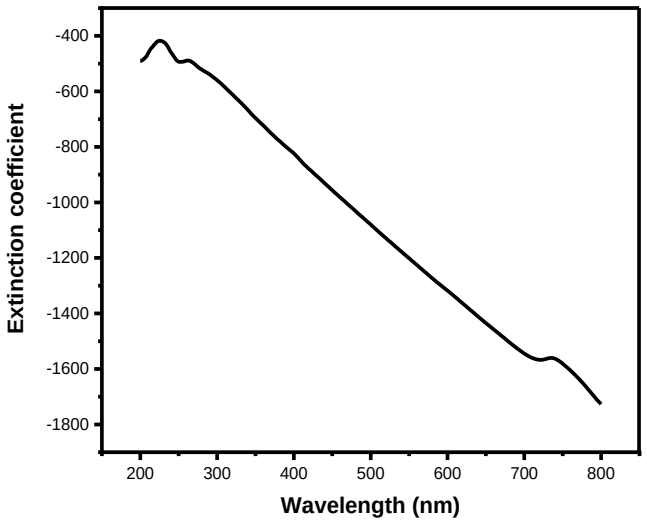

Fig.3 (d) UV-vis Extinction coefficient

The optical extinction coefficient of the sample was evaluated via UV-vis spectroscopy across the wavelength range, showing a wavelength-dependent variation indicative of the material's light absorption characteristics.

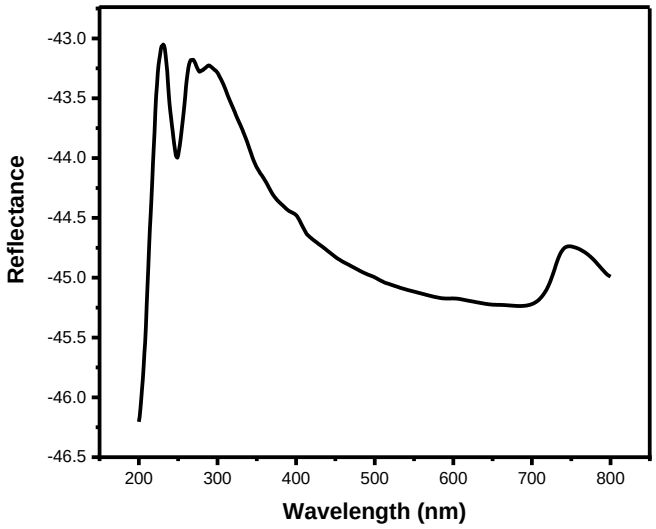

Fig.3 (e) UV-vis Reflectance

The reflectance profile has been measured for the purpose of examine its light response from the crystalline sample. In Ultraviolet-visible reflectance measurements, the reflectance (%) represents the fraction of incident light reflected by the material when exposed to ultraviolet and visible light. It helps to understand the optical properties, band gap, and surface characteristics of powder samples. A lower reflectance indicates higher absorption of light by the material.

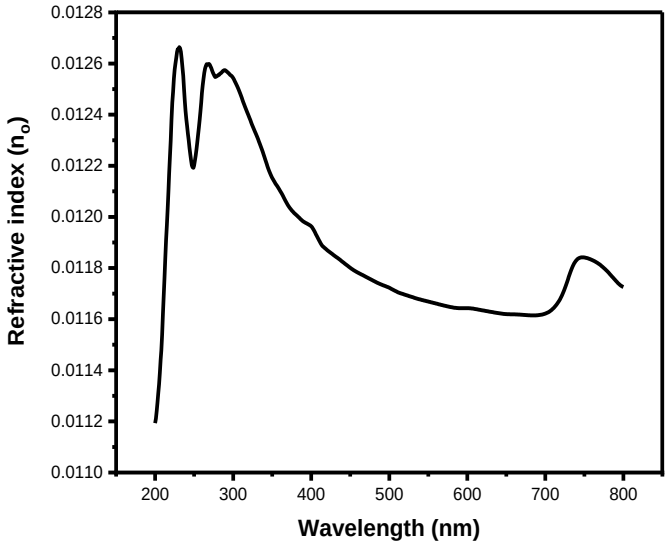

Fig.3 (f) UV-visible Refractive index

The Refractive index (n_o) was derived through absorption spectra, providing information on the light propagation within the material. The refractive index for sample is determined using UV-vis spectra across the wavelength range, showing a gradual variation with wavelength, which reflects the material's optical dispersion characteristics.

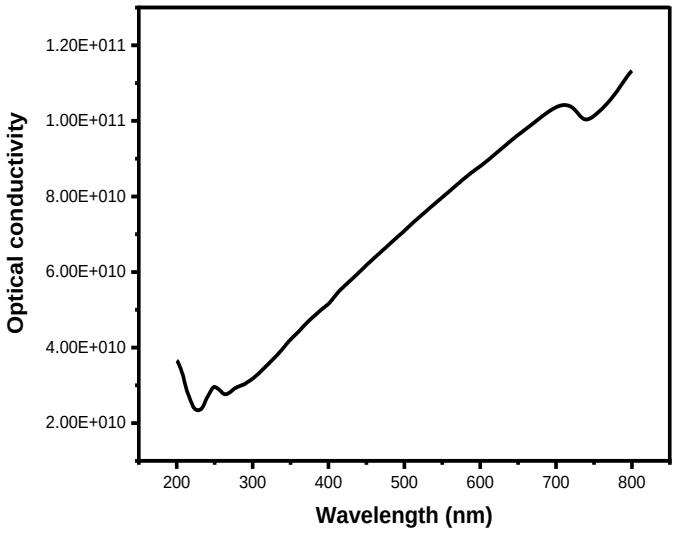

Fig.3 (g) UV-vis optical conductivity

The optical conductivity was calculated to understand the interaction of photons with charge carries in the material. The optical conductivity of the material is evaluated through Ultraviolet-visible spectroscopy, showing a wavelength-dependent behaviour that reflects the material's electronic and optical properties **[16, 17]**.

4). SEM analysis

SEM is an effective method employed for examining the surface topography and microstructural features of crystalline samples. It provides high-resolution micrographs that reveals the morphology, dimensions, and spatial arrangement of particles, grain or layers, as well as any defects such as cracks, voids or irregularities. Through SEM, the uniformity, compactness, and overall structural integrity of the sample can be effectively assessed.

SEM was conducted to investigate the surface topography from the as synthesized material **[18]**. The micrographs revealed a well-defined surface with uniform texture, indicating good crystalline quality. The absence of visible grain boundaries or cracks

confirms the homogeneity of the material, while the observed surface features provide insight into the growth mechanism and defect distribution **[19]**.

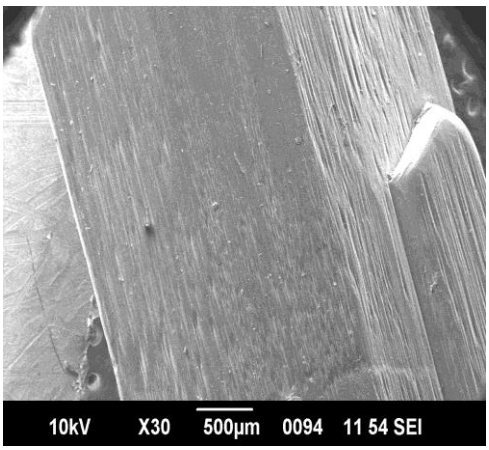

Fig.4 (a). Photograph of SEM

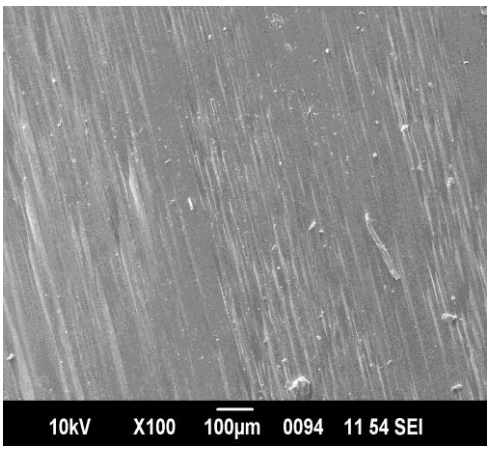

Fig4 (b). Photograph of SEM

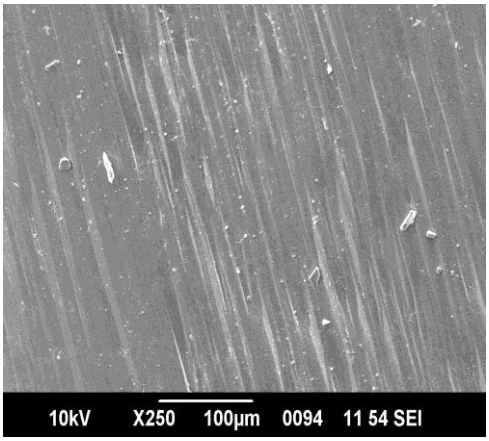

Fig.4 (c). Photograph of SEM

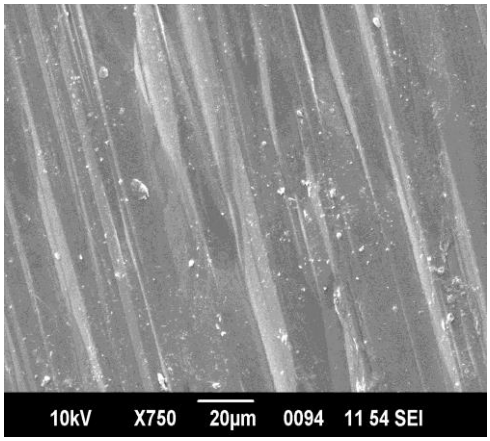

Fig.4 (d). Photograph of SEM

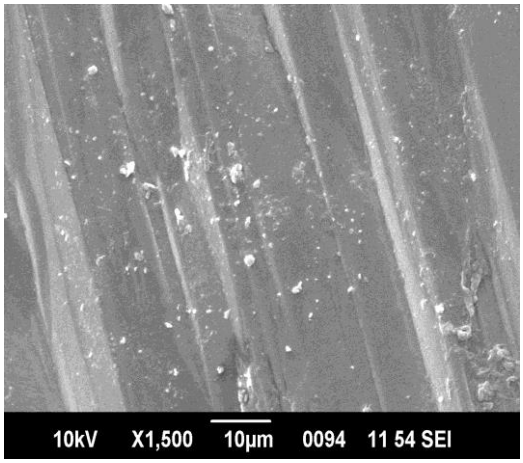

Fig.4 (e). Photograph of SEM

5). CHN analysis

CHN characterization is performed to determine the elemental content of the synthesized sample in terms of carbon (C %), hydrogen (H %), and Nitrogen (N %) content **[20, 21]**. The experimental values were compared with the theortical stoichiometric percentages to confirm the chemical purity and proper molecular composition of the material **[22]**. Elemental analysis (CHN) indicated that the sample comprised Carbon (40.64 %), Hydrogen (7.44 %) and Nitrogen (10.71 %) of the sample's total weight, respectively **[23]**. The results indicated close conformity with the expected results, verifying the absence of unwanted impurities. Accurate elemental composition is crucial for NLO crystals, as deviations can affect the crystal structure, optical quality and efficiency in nonlinear optical applications **[24, 25]**.

Table. (2) CHN elemental composition of the sample

Sample weight	Carbon (%)	Hydrogen (%)	Nitrogen (%)
7.60	40.64	7.44	10.71

6). Photoluminescence analysis

Photoluminescence studies were conducted to examine the emission characteristics in the synthesized material **[26]**. The sample was excited with a suitable wavelength, and the emitted light was recorded to study its electronic transitions and defect states **[27]**. The PL spectrum revealed sharp and well-defined emission peaks, indicating high optical quality and minimal structural defects **[28]**. Such optical behaviour is critical for nonlinear optical (NLO) functionalities, since it reflects the efficiency of light-matter interaction, transparency and suitability for frequency conversion or laser based devices **[29]**. The intensity and position of the emission peaks also provide insight into the electronic band structure and potential energy level within the material.

$$E_g = 1240 / \lambda \qquad (1)$$

The biggest peak produced at 466 nm arises from the hydroxyl (-OH) group, and the electronic transitions responsible is (n-σ*). The other peaks are observed at 536 nm and 822 nm. At sharp peak of 466 nm to corresponds to 2.66 eV photoluminescence of L-Threonine renders it promising for candidate for nonlinear optical applications including optical switching and frequency conversion in photonic applications **[30, 31]**.

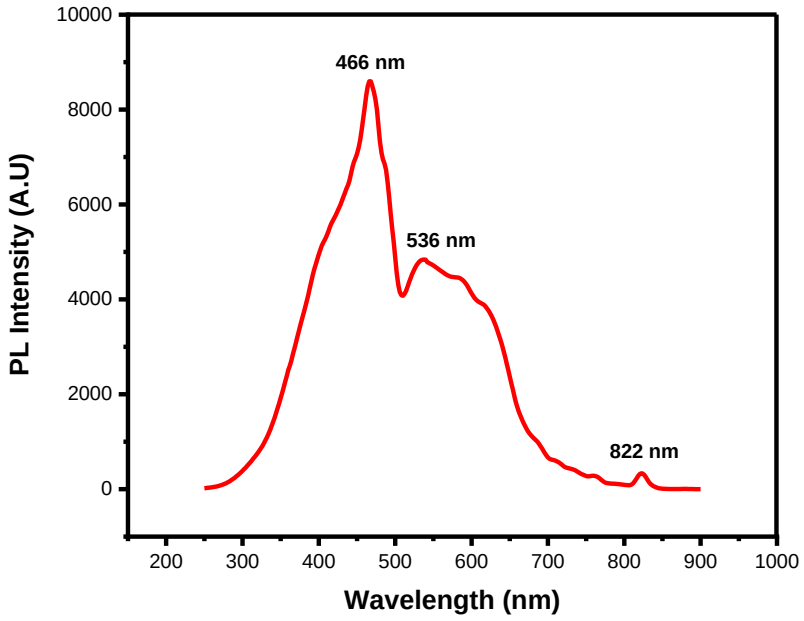

Fig (6). PL Emission profile of L-Threonine single crystals

7). Energy dispersive energy analysis

Energy dispersive X-ray (EDX) method was performed for examining the elemental constituent within the specimen. The technique allowed precise identification of the elements present and their relative concentrations. Data obtained from EDX yielded significant information regarding the chemical uniformity of the material. The analysis confirmed the presence of all expected elements without detectable contamination **[32]**. EDX spectra were recorded and analyzed to quantify the elemental ratios accurately. This method also offered information about the distribution of elements across the sample surface. The results were consistent with the nominal chemical formula of the material. Elemental mapping further highlighted regions of uniform composition. The finding from EDX supported complementary characterization techniques. Overall, EDX proved to be a reliable tool for elemental verification and compositional analysis **[33]**.

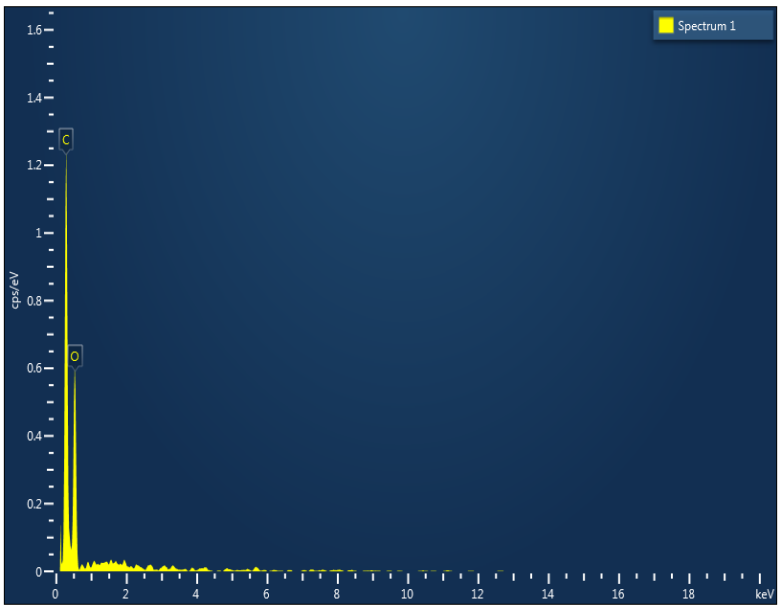

Fig. (7) Energy dispersive X-ray (EDX) profile of the sample

Table. (3)

Elemental constituents in the material were analyzed using Energy dispersive x-ray technique

Element	Line Type	Wt %	Atomic %
C	K series	54.09	61.08
O	K series	45.91	38.92
Total:		**100**	**100**

8). Z scan in liquid analysis

Z-scan analysis is highly reliable and well-established method for investigating nonlinear optical (NLO) characteristics for the sample. It involves translating a sample along the propagation axis (z-axis) of a converged laser beam while measuring the transmitted signal relative to its spatial location **[34]**. This method provides quantitative information about both the nonlinear optical refractive index (n_2) and the nonlinear optical absorption coefficient (β) of a material.

This method enable concurrent determination of the nonlinear optical Refractive index (n_2) and nonlinear optical absorption coefficient (β) under high-intensity light. within this method, the specimen is moved along the axis within a converged beam irradiation. Depending on the measurement, detector records the emergent light through an aperture (closed aperture Z-scan) to detect refractive index changes or without an aperture (open aperture Z-scan) to study nonlinear optical absorption phenomena such as saturable and reverse saturable absorption. Nonlinear refraction provides information on intensity-dependent changes in the refractive index of the material **[35]**.

By fitting experimental data to theoretical models, key quantities including the nonlinear optical refractive index (n_2) along with the Nonlinear optical absorption (β) can be evaluated accurately. The Z-scan technique can be considered simple, sensitive, and requires minimal sample preparation. It is widely used to characterized sample such as optical switching, photonic devices, and laser protection, helping researchers understand light-matter interactions at high intensities. Overall, the Z-scan provides a straightforward and reliable approach for characterizing nonlinear optical materials.

In this Research work, the Z-scan experiment were performed by a laser operating at a wavelength of 632.8 nm laser with a power (E_p) of 12.0 mW and a beam diameter (d) of 5mm, focused through a 200 mm lens onto a 1 mm thickness sample (L), with a sweeping

distance of 40.0 mm and a step size of 0.5mm. The system featured a high-bandwidth configuration, with an aperture radius of 2mm, the radius of the beam at the aperture (W_a) of 4.5 mm, a sample linear refractive index (n_o) of 1.5, and a transmittance of 70%.

The sample thickness (L) was measured to be 1mm, while the Rayleigh length (Z_R) for the focused laser light was calculated as 1.29 mm. since $L < Z_R$, the beam remained effectively collimated within the sample during the Z-scan experiment. The sample was positioned onto an automated linear positioning platform, and the incident laser beam travelled from the negative (-Z) region toward the positive (+Z) region.

Z-scan experiment were examined using third-order nonlinear optical behaviour of the synthesized crystal. The open-aperture curve confirmed the existence of nonlinear optical absorption processes, while the closed aperture curve revealed a self-focusing nonlinear optical refractive index. Form the experimental data, the nonlinear optical coefficients were evaluated, indicating the crystal's strong interaction with intense laser radiation **[36]**.

The nonlinear optical characterization of the material were investigated via the Z-scan method. In the closed aperture measurement, the peak transmittance T_p is 0.0033 and valley transmittance T_v is 0.0029 yielded a transmittance difference of ΔT_{p-v} is 0.0004 from which the nonlinear optical refractive index (n_2) has been determined.

In the open aperture configuration, the peak T_p is 0.0092 and valley T_v is 0.0086 transmittance resulted in a minimum transmittance differences of ΔT_{min} is 0.9914 indicating the existence of a significant nonlinear optical absorption coefficient (β) within the material.

The open aperture Z-scan curve exhibited a valley to peak shape, with the lowest transmission intensity occurring near the beam waist (z=0), indicating occurring at the focal point (RSA) behavior within the material. The positive nonlinear optical absorption

coefficient (β >0) demonstrates the material's applicability to optical limiting and other nonlinear photonic applications.

The closed aperture Z-scan curve displayed a valley to a peak profile, with the peak and valley transmittance occurring near the beam waist (z=0), suggesting a positive nonlinear optical refractive index (n_2>0) and self-focusing behaviour in the sample, with applications primarily in nonlinear photonics, including all optical switching.

The Nonlinear optical characteristics exhibited by the specimen was examined through the Z-scan experiment. The nonlinear optical refractive index (n_2) was calculated as 4.39 x 10^{-15} m^2/W, and the nonlinear optical absorption coefficient (β) was found 5.66 x 10^{-5} m/W. From these parameters, the third order nonlinear optical susceptibility has been determined, yielding a real part Re ($X^{(3)}$) is 2.50 x 10^{-13} esu. An imaginary part Img ($X^{(3)}$) is 1.62 x 10^{-8} esu, and a magnitude of third order susceptibility $|X^{(3)}|$ is 1.62 x 10^{-8} esu, indicating a material demonstrate notable third-order nonlinear optical behavior.

Z-scan experiment demonstrated that the crystal's pronounced third-order nonlinear optical susceptibility, indicating its potential for optical limiting, all optical switching and Photonic devices **[37, 38]**.

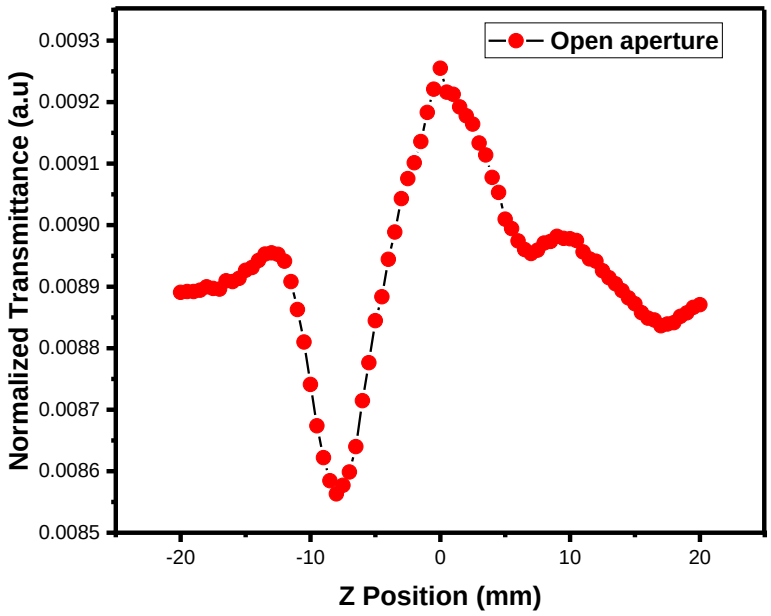

Fig.8 (a). Z scan - Open aperture

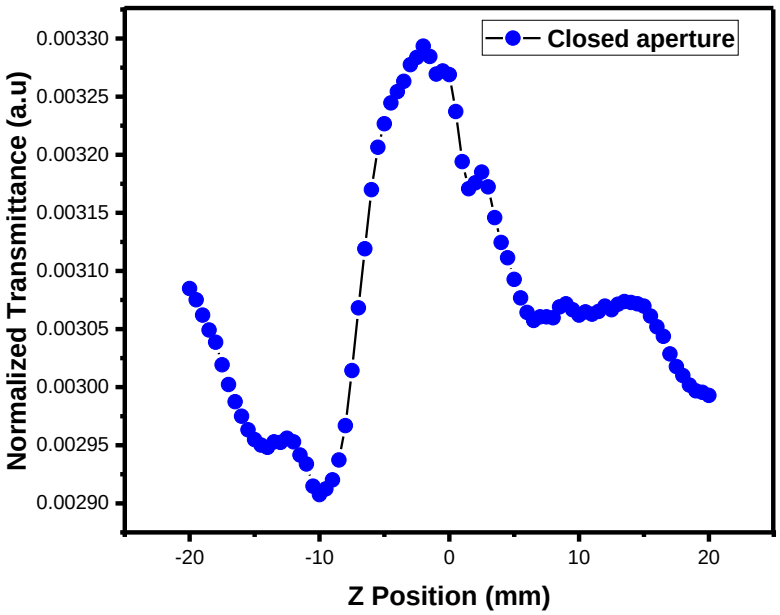

Fig.8 (b). Z scan - Closed aperture

9). Antibacterial test

In this study, the antibacterial properties of crystals grown from the synthesized organic compound were systematically investigated to evaluate their potential biomedical applications **[39]**. The crystallization process was optimized to obtain high-purity, well-defined single crystals, which were then subjected to anti bacterial testing towards a set of gram-positive and gram-negative bacteria **[40]**. The analysis involved determining the inhibition zones, minimum inhibitory concentrations (MIC), and potential bactericidal effects, allowing for a thorough evaluation regarding crystallinity, topographical features, and molecular arrangement of the crystals influence their antibacterial activity **[41]**. By correlating the structural characteristics of the grown crystals with their biological efficacy, this investigation offers critical understanding of the design of functional crystalline substances exhibiting enhanced antimicrobial characteristics, that could be useful in pharmaceutical and biomedical applications.

The antimicrobial activity exhibited by the tested sample was assessed involving two bacterial species, S. aureus (Gram-positive) and E. coli (Gram-negative), through the standard disc diffusion assay. The control samples exhibited clear inhibition zones of 25 mm for both bacterial strains, confirming the validity of the experimental setup **[42]**. In, contrast, the tested sample did not exhibit any observable zone of inhibition against either S. aureus or E. coli, suggesting that under the experimental conditions employed, the sample lacked detectable antibacterial activity. These results indicate that the sample was ineffective in suppressing the proliferation of the tested gram positive and gram negative bacteria and may require further modification or testing under different conditions to evaluate its potential antimicrobial properties **[43]**.

Fig.9 (a). Antibacterial activity – S. Aureus **Fig.9 (b). Antibacterial activity – E. coli**

Table. (4)

Antibacterial efficacy of L-Threonine showing no inhibition against the tested bacterial strains.

S.NO	Strain	Gram reaction	Control	Zone of inhibition (mm)
1.	S. aureus	+ Gram	25	NIL
2.	E. Coli	- Gram	25	NIL

10). TG-DTA studies

The TG-DTA analysis and DTG studies were performed from 10°C–750°C under a nitrogen atmosphere. Thermogravimetric and differential thermal studies were performed on L-Threonine single crystals with a sample mass of 7.511 mg to examine their thermal stability and phase transition behaviour **[44]**.

The DTA measurements were recorded as heat flow with the endothermic direction downward (Mw), revealing multiple endothermic events at 198.86℃, 219.38℃, 234.88℃,

253.86℃, 286.59℃, 329.77℃, and 422.73℃. These transitions indicate stepwise thermal processes, which may correspond to lattice reorganization, partial melting, or other structural relaxations within the crystal lattice **[45, 46]**.

Furthermore, glass transition temperatures TG (mg) were identified at 236.62℃, 286.59℃, and 538.16℃, representing discrete regions of molecular mobility and structural relaxation. The observed thermal events suggest that the L-Threonine single crystals remain temperature dependent stability up to approximately 198℃, with subsequent endothermic peaks reflecting gradual structural modifications and decomposition processes. The detailed TG-DTA profile thus provides a comprehensive understanding of the thermal characteristics of L-threonine single crystals, including both their stability and phase transition behaviour under controlled heating conditions **[47]**.

The derivative thermogravimetry (DTG) analysis revealed a major peak at 251.62°C, representing the point of highest mass-loss rate, and a smaller weight loss at 268.85°C, indicating a slower secondary decomposition process. These observations highlight distinct stages of thermal degradation, providing valuable insight into the heat induced stability and degradation kinetics for the material.

The thermal degradation kinetics for the material were analyzed using TG-DTA, and both the broidos and Kissinger methods were employed to evaluate the kinetic parameters. The broido method provided a deeper understanding of the stepwise characteristics of the decomposition process, capturing subtle variations in reaction kinetics, whereas the Kissinger method offered a simpler and rapid estimation of the activation parameters. Both methods yielded consistent trends in describing the thermal behaviour, highlighting the reliability of the kinetic analysis and demonstrating that the combination these approaches enables a thorough elucidation of the material's stability and decomposition mechanism **[48]**.

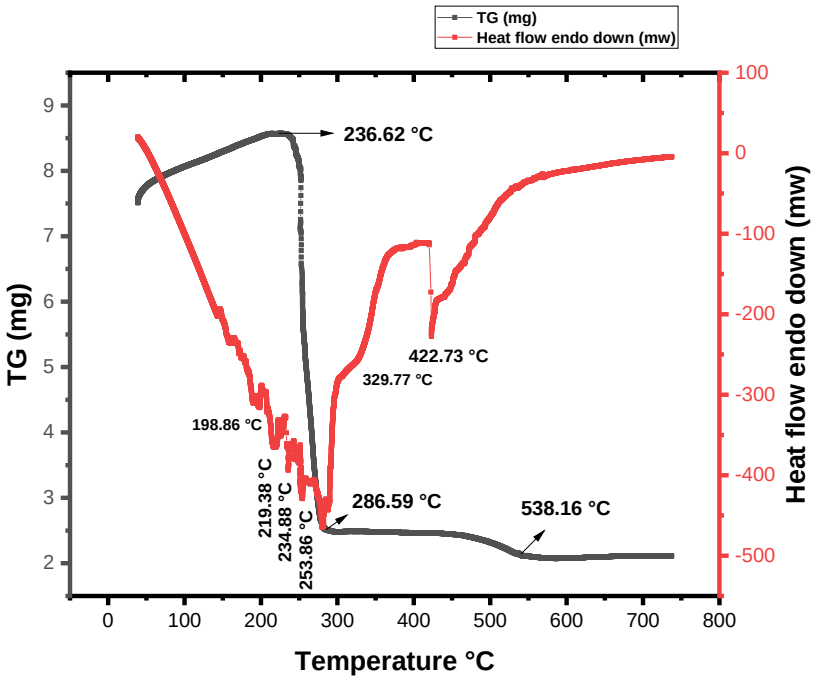

Fig 10 (a). DTA curve showing TG of the sample weight (%) vs Heat heat flow endo down

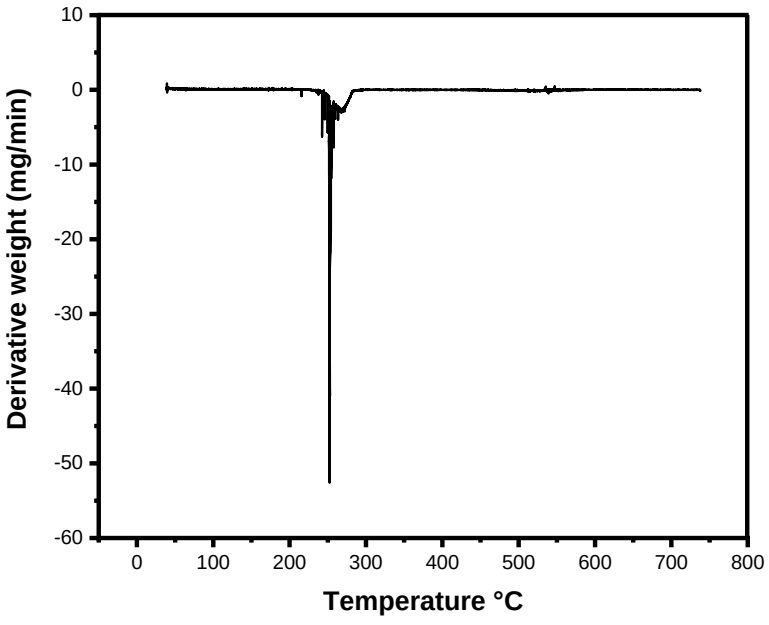

Fig 10 (b). DTG curve: Temperature (°C) vs derivative weight (mg/min)

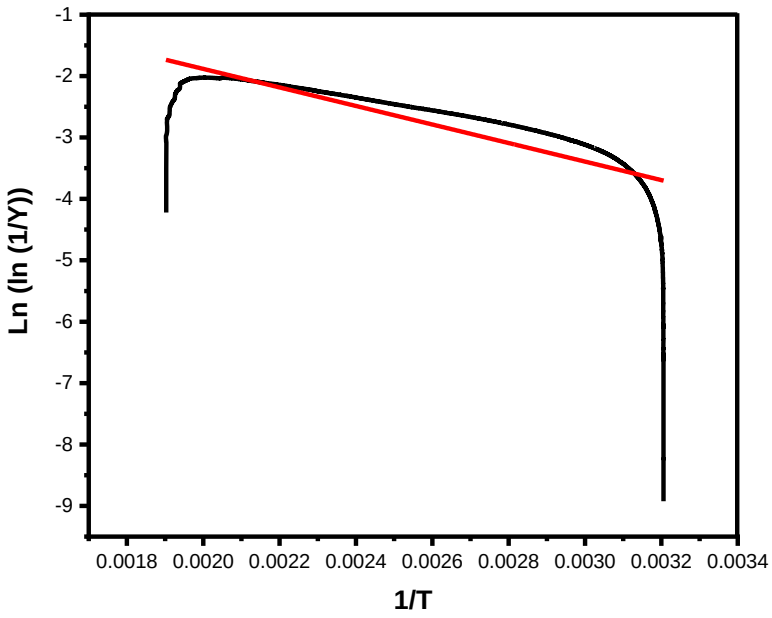

Fig 10 (c). Thermal analysis of the sample using the Broidos method

Table. 5

Kinetic thermal parameters of Broidos method

Kinetic parameters	**Values**
Slope	-1509.7329
Temperature in Kelvin	321.543
Frequency factor in (A) sec^{-1}	5.03 x 10^2 sec^{-1}
Activation energy (Ea) in J/mol^{-1}	12554
Entropy of activation (ΔS) in J/mol^{-1}	-275.1

Enthalpy of activation (ΔH) in J/mol^{-1}	9882
Gibbs free energy (ΔG) in J/mol^{-1}	98336

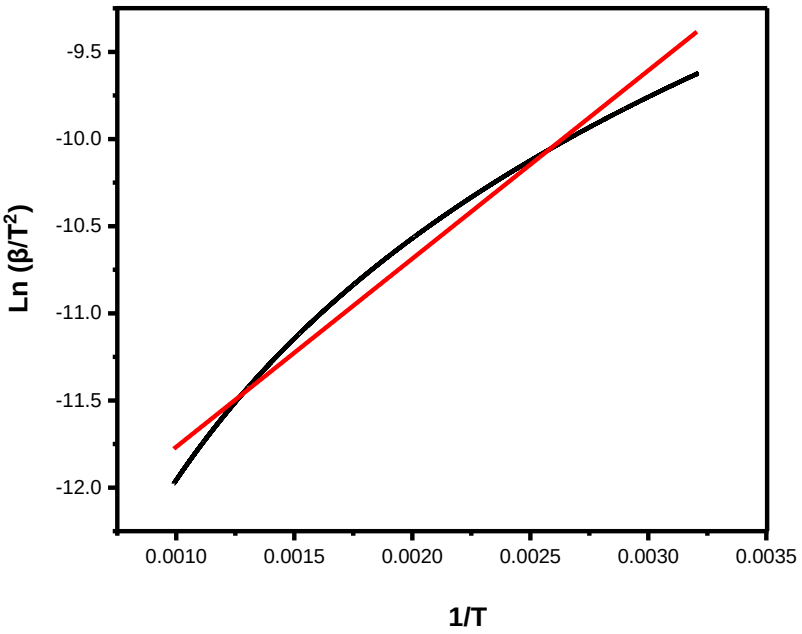

Fig 10 (c). Thermal analysis of the sample using the kissinger method

Table. 6

Kinetic thermal parameters of kissinger method

Kinetic parameters	**Values**
Slope	1079.6626
Temperature in Kelvin	476.19

Frequency factor in (A) sec^{-1}	2.86 x 10^{-3}
Activation energy (Ea) in J/mol^{-1}	8968.9
Entropy of activation (ΔS) in J/mol^{-1}	-298
Enthalpy of activation (ΔH) in J/mol^{-1}	5011.6
Gibbs free energy (ΔG) in J/mol^{-1}	146811.6

---

11). Fourier transform nuclear magnetic resonance

1H FT-NMR

The 1H FT-NMR characterization performed on the prepared material displayed several characteristic resonances in the region of δ 4.140- 4.078ppm, which are assigned to the methane (-CH) and Hydroxymethylene (-CH-OH) protons of the amino acid backbone. Additional peaks observed at δ 3.447 and 3.435 ppm correspond to protons bonded to the carbon atom bearing the hydroxyl functionality, confirming the detection of the β- hydroxyl chemical moiety of the sample **[49, 50]**. The signals at δ 1.189 and 1.172 ppm arise from the terminal methyl protons, validating the aliphatic side-chain environment characteristic of threonine

13C FT-NMR

The 13 C FT NMR spectrum exhibited a distinct resonance at δ 175.75 ppm, assigned to the carboxyl carbon (C=O) to the amino group. The signals observed at δ 65.80 and 60.31 ppm is associated with the β- carbon bonded to the hydroxyl group and an α-carbon linked with an amino group , respectively, confirming the characteristic carbon skeleton of L-Threonine.

The Low-field aliphatic carbon peaks at δ 19.40 and 19.36 ppm are assigned to the terminal methyl carbon atoms **[51]**.

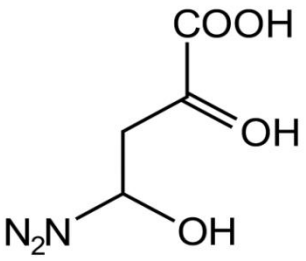

Fig 11. Molecular structure for L-Threonine single crystals

1H FT NMR

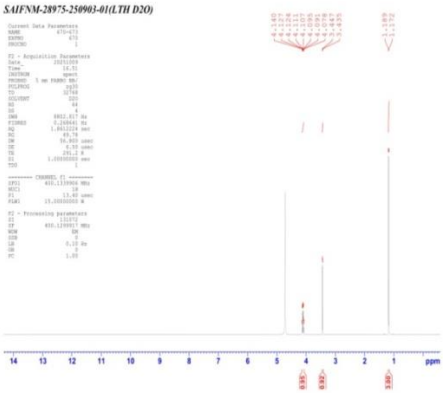

Fig. 11 (a) 1H FT-NMR

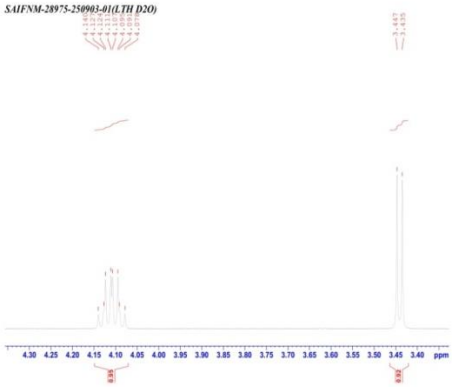

Fig. 11 (b) 1H FT-NMR

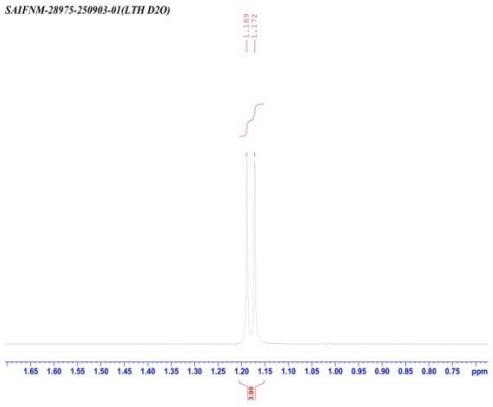

Fig. 11 (c) 1H FT-NMR

13C FT-NMR

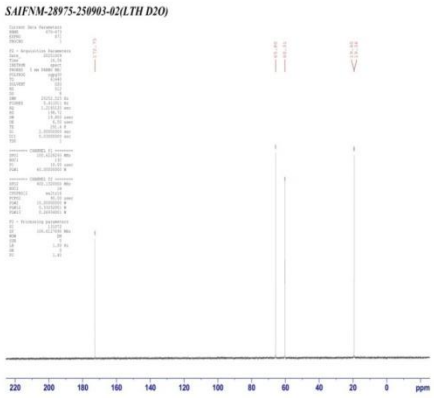

Fig. 11 (d) 13C FT NMR

12). Microhardness

The microhardness of the sample were recorded under applied loads of 25, 50, 75, 100 gm yielding hardness values (H_v) of 28.58, 52.07, 42.17, and 55.12 kg/mm^2, respectively, which demonstrates a nonlinear dependence of hardness on the indentation load**.** The hardness in the material initially rises under the applied load, then shows a slight decrease,

followed by a further increase at higher loads, reflecting a nonlinear dependence characteristic of the indentation size effect (ISE). The measured variation of load-dependent microhardness is indicative the indentation size effect (ISE), a widely recognized phenomenon in crystalline materials where load dependent varies with the applied load and corresponding indentation size **[52]**.

The indentation diameters of the grown crystals was determined at Log P (g) of 1.398, 1.699, 1.875, and 2, corresponding to indentation diameters of 1.605, 1.625, 1.759, and 1.763 μm, respectively, demonstrating a gradual increase in indentation size with increasing load. The microhardness of the sample was evaluated, and the mayer's index (n) value has observed 2.79, indicating the material's hardness characteristics under the applied load. The variation in load-dependent hardness as a function of indentation load confirms a clear indentation size effect (ISE), since the measured microhardness values change non-linearity with increasing load, reflecting the effect of indentation size on mechanical strength of the material **[53]**.

The load-dependent change in the stiffness coefficient (C11) under applied load (P) is analyzed for evaluating the elastic behaviour of the synthesized crystal. The variation with applied Load (P) and the stiffness coefficient (GPa) reveals the stiffness rises with applied load, indicating the strong bonding nature and enhanced resistance to deformation under higher applied stress. This behaviour demonstrates the good elastic resistance of the material **[54]**.

The relationship with applied load (P) and Yield strength (MPa) was examined to assess the elastic performance of the synthesized material. The yield strength was found to vary with increasing load, indicating that the material exhibits good resistance to plastic

deformation under higher applied stresses. This variation suggests the strong bonding nature and structural stability of the crystal **[55]**.

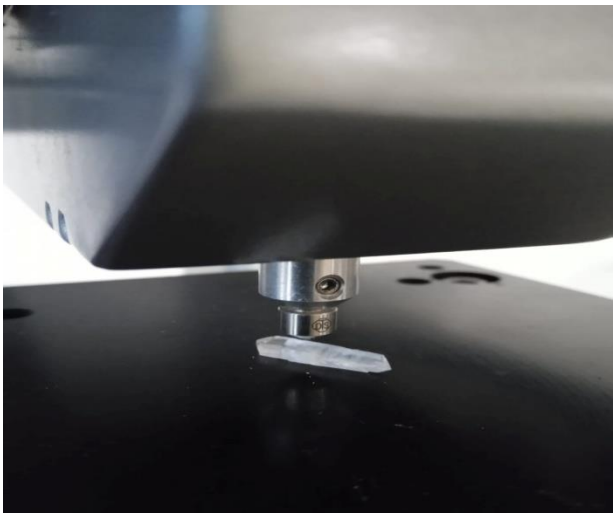

Fig. 12 (a). Photographic image showing the mechanical strength of the L-Threonine crystal

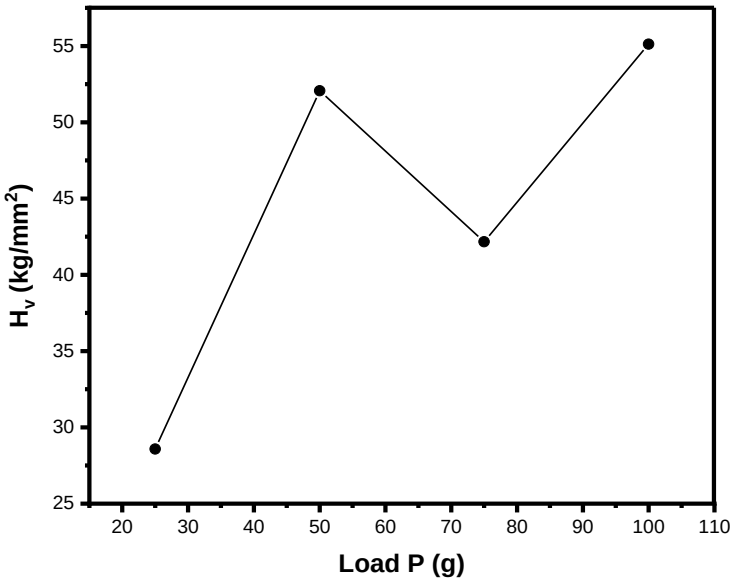

Fig.12 (b). Load P (g) versus Hv (kg/mm^2)

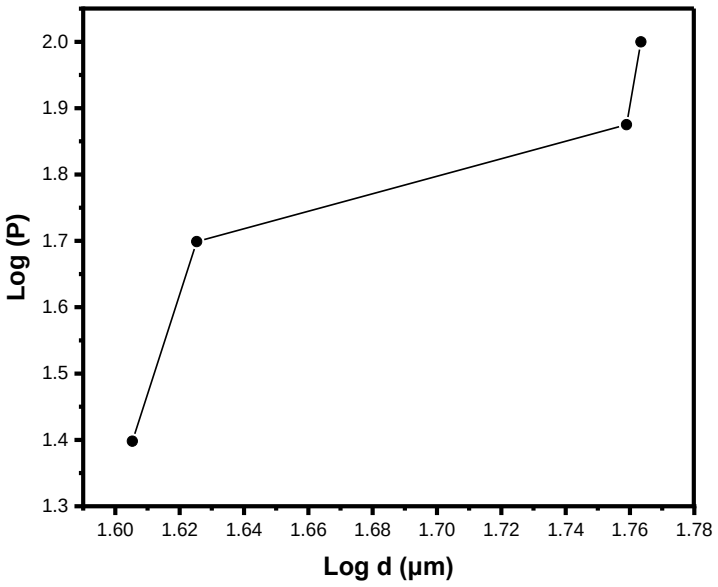

Fig.12 (c). Log d (µm) versus Log P (g)

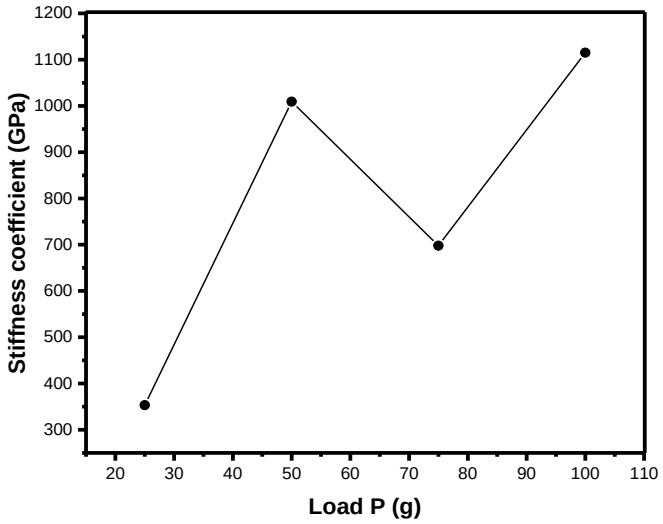

Fig.12 (d). Load P (g) versus Stiffness coefficient (GPa)

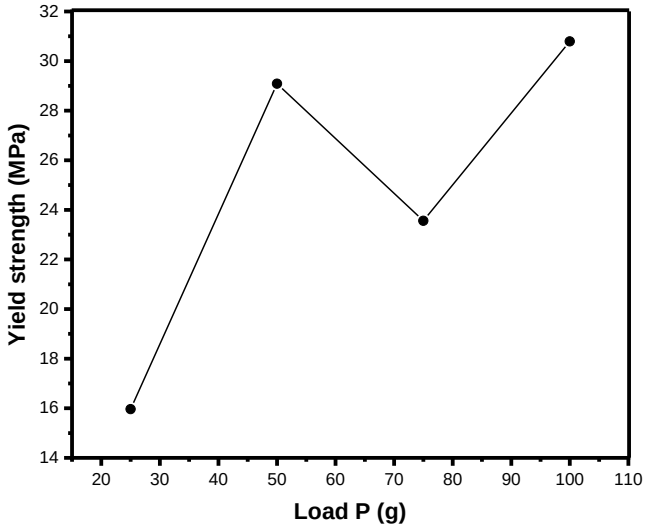

Fig.12 (e). Load P (g) versus Yield strength (MPa)

Conclusion

In powder XRD the various parameters of a = 7.738 A°, b= 13.62 A°, c = 5.137 A° and these three angles correspond to $\alpha = \beta = \gamma = 90°$ and the crystal crystallizes in an orthorhombic system with a primitive lattice, belonging to the space group $P2_12_12_1$. Fourier transform infrared studies confirmed the characteristic chemical groups, ensuring the molecular group assignments and purity of the grown material. Ultraviolent-visible studies facilated the evaluation of absorbance, Transmittance is 90 %, Direct band gap (Tauc plot) is 4.60 eV, Refractive index, Reflectance, optical conductivity and Extinction coefficient there by providing comprehensive insight into the optical and opto-electronic characteristics of the material. SEM analysis revealed a uniform surface morphology with well defined facets, indicating the structural quality of the crystal. The evidenced elemental peaks are consistent with the constituent atoms, indicating the successful incorporation of all components and the absence of significant impurities. CHN analysis confirmed that the carbon (40.64 %), Hydrogen (7.44 %), and Nitrogen (10.71 %) content of the synthesized crystal closely

matches the theortical values, indicating the purity and correct stoichiometry of the material. The strong and maximum peak observed around the 466 nm and the electron excitation band-gap (E_g) was measured to be 2.66 eV. Z-scan studies confirmed the NLO response of the sample, with a third-order NLO susceptibility of 1.26 x 10^{-9} esu, indicating its potential for optical limiting, optical switching, optical modulation and data storage. The mayer index (n) for microhardness was found to be 2.79, classifying the material in the hard category. The Load (P) versus hardness, stiffness, and yield strength analysis shows that the material resists deformation effectively, this indicates good mechanical stability. The 1H and 13C FTNMR analyses of L-Threonine single crystals successfully confirmed the expected proton and carbon environments, including α- and β-Protons, methyl groups, and the carboxyl carbon. These results validate the molecular framework of L-Threonine and demonstrate the effectiveness of FT-NMR in detailed structural characterization of amino acid crystals. The antibacterial studies demonstrated no inhibition of the tested bacterial strains, indicating that the material is inactive against these bacteria. The temperature-dependent behaviour of the sample was analysis using DTA and DTG analyses, which showed a Thermogravimetric analysis (TG) at 198.86℃ and a sharp DTG peak at 250℃, while the rate parameters of decomposition were evaluated by both the Kissinger and broidos methods, providing insight into the material's thermal stability and decomposition mechanism.

References

[1]. N. Rajasekar, K. Balasubaramanian. Exploring structural, spectroscopic, Optical, Morphological, Mechanical, Antibacterial and Thermal parameters of Glycine A.R single crystals for advanced opto electronics, Photonics, Laser components and Nonlinear optical applications. Journal of nanotechnology perceptions (www.nano-ntp.com). 20 No. S 14 (2024), 4857-4893.

ISSN 1660-6795.

DOI : https://doi.org/10.62441/nano-ntp.vi.5784

[2]. G. Ramesh Kumar, S. Gokul Raj, R. Mohan, and R. Jayavel. Influence of Isoelectric pH on the Growth Linear and Nonlinear Optical and Dielectric Properties of L-Threonine Single Crystals. Crystal Growth & Design, Vol. 6, No. 6, 2006

[3]. G. Ramesh Kumar, S. Gokul Raj, Amit Saxena, A.K. Karnal, Thenneti Raghavalu, R. Mohan, Deuteration effects on structural, thermal, linear and nonlinear properties of l-threonine single crystals, Materials Chemistry and Physics. 108, (2008), 359–363.

DOI :10.1016/j.matchemphys.2007.10.015

[4]. N. Mahalakshmi, M. Parthasarathy, Growth, Spectral, Optical, Dielectric, Laser Damage Threshold and Second Harmonic Generation studies of L-Threonine single crystals for Potential nonlinear optical applications, Eur. Chem. Bull. (2023), 12 (Special Issue 4), 14011-14026.

DOI: 10.48047/ecb/2023.12.si4.1271

[5]. G. Ramesh Kumar, S. Gokul Raj, R. Shankar, R. Mohan, R. pandi and R. Jayavel, Growth structural, Optical and Thermal studies of Non-Linear optical L-Threonine single crystals. Journal of crystal growth. 267, (2004), 213-217.

DOI :10.1016/j.jcrysgro.2004.03.073

[6]. G. Ramesh kumar, S. Gokul Raj, R. Mohan, R. Jeyavel, Growth, Structural and spectral analyses of Non linear optical L-Threonine single crystals. Journal of crystal growth. 275, (2005), e1947-e1951.

DOI :10.1016/j.jcrysgro.2004.11.283

[7]. A. Hemalatha, S. Arulmani, P. Sanjay, K. Deepa, J. Madhavan and S. Senthil. Growth and Characterization of L-Leucenium Hydrogen Maleate Single Crystals for Nonlinear Optical Applications. IOP Conf. Series: Materials Science and Engineering. 360, (2018), 012044.

DOI : 10.1088/1757-899X/360/1/012044

[8]. D. Subashini, A. R. Prabhakaran, S. Nalini Jayanthi and K. Thamizharasan. Spectral, thermal investigations and particle size determination of L-threonine single crystals. Advances in Applied Science Research. 2013, 4(2):238-242

[9]. G. Thilagavathi, R. Arun Kumar, V. Gunasekaran. Influence of L-threonine on the growth, structural, optical, mechanical and nonlinear optical properties of tartaric acid single crystal. Materials Science-Poland, 36(4), 2018, pp. 630-637

DOI: 10.2478/msp-2018-0094

[10]. K. Kanagasabapathy, R. Rajasekaran. Growth, structural, optical and thermal studies of L-Threonine added Zinc (Tris) Thiourea Sulphate single crystals. Journal of Optoelectronics and Advanced Material. Vol. 6, No. 1-2, January-February 2012, p. 218 - 224

[11]. T. Kalaiarasi, M. Senthilkumar, S. Shanmugam, T. Jarin, V. Chithambaram, Kishor kumar sadasivuni and M. Nagarajan. Synthesis and characterization of L-threonine ammonium bromide: grown on single crystal with experimental studies on NLO. Bull. Mater. Sci. (2021) 44:175

DOI : https://doi.org/10.1007/s12034-021-02421-6

[12]. S. E. Allen Moses, S. Tamil selvan, S. M. Ravikumar, G. Vinitha, Tejaswi Ashok hedge, M. Vimalan, S. Varalakshmi, S. Sivaraj. Synthesis growth and physiochemical properties of new organic nonlinear optical crystal L-Threonium tartarate (LTT) for frequency conversion. Journal of Materials Science for Energy Technologies, 2 (2019) 565–574

DOI : https://doi.org/10.1016/j.mset.2019.05.003

[13]. G. Ramesh kumar, S. Gokul Raj, R. Mohan, R. Jeyavel. Growth and characterization of new nonlinear optical L-Threonium acetate single crystals. Journal of crystal growth 283 (2005) 193-197.

DOI : 10.1016/j.jcrysgro.2005.04.103

[14]. C. Deepa, M. Anbuchezhiyan. Evolving NLO effect, Mechanical, thermal and dielectric study of N- Benzoyl glycine doped L- Threonine. Materials Today: Proceedings

DOI : https://doi.org/10.1016/j.matpr.2020.11.590

[15]. R. Purusothaman , M. Shankar , A. Dennis Raj , M. Vimalan , and I. Vetha Potheher. A study on NLO, ultraviolet transparency, photoconductivity, and dielectric response of organic single crystal. J Mater Sci: Mater Electron (2023) 34:2292.

DOI : https://doi.org/10.1007/s10854-023-11691-1

[16]. Mohd. Shkir, V. Ganesh, S. AlFaify, H. Algarni, G. Bhagavannarayana, K. K. Maurya, M. M. Abutalib and I. S. Yahia. Bulk growth, structural, vibrational, crystalline perfection, optical and dielectric properties of L-threonine doped KDP single crystals grown by Sankaranarayanan-Ramasamy (SR) method. Materials Research Innovations. 14 June 2016. ISSN: 1432-8917

DOI : 10.1080/14328917.2016.1192715

[17]. Sagadevan suresh. Synthesis, growth and characterization of L-Threonine zinc acetate (LTZA) NLO single crystal. Journal of optik. Int. J. Light Electron Opt. (2014).

DOI : http://dx.doi.org/10.1016/j.ijleo.2014.02.008

[18]. Redrothu Hanumantha Rao, S. Kalainathan, Microhardness, chemical etching, SEM, AFM and SHG studies of novel nonlinear optical crystal – L-Threonine formate. Material research bulletin 47 (2012) 987-992

DOI : 10.1016/j.materresbull.2012.01.013

[19]. J. Elberin mary theras, D. Kalaivani, J. Arul martin mani, D. Jeyaraman, V. Joseph. Synthesis structural and optical properties, ferromagnetic behaviour, cytotoxicity and NLO activity of lithium sulphate doped L-Threonine. Journal of Optics & Laser Technology 83 (2016) 49–5450

DOI : http://dx.doi.org/10.1016/j.optlastec.2016.03.027

[20]. G. Thilakavathi, R. Arun Kumar, V. Gunasekaran. Influence of L-threonine on the growth, structural, optical, mechanical and nonlinear optical properties of tartaric acid single crystal. Materials Science-Poland, 36(4), 2018, pp. 630-637.

DOI: 10.2478/msp-2018-0094

[21]. S. Anna Venus, S Anbarasu , Prem Anand Devarajan. Studies on the synthesis, growth and physic - chemical properties of a new single NLO crystal: potassium L-threoninate. International Journal of Recent Trends in Science And Technology, Volume 10, Issue 3, 2020 pp 01-07. ISSN 2277-2812.

[22]. I. Vetha Potheher , K. Rajarajan , M. Vimalanc , T. Rajesh Kumar , R. Jeyasekaran and P. Sagayaraj. Investigation on the Growth and Characterization of Nonlinear Optical Single Crystals of Tris-Allyl Thiourea Mercury Bromide (ATMB). Archives of Applied Science Research. 2010, 2 (3): 171-182.

[23]. B. Narayana Moolya, S.M. Dharmaprakash. Synthesis, growth and characterization of nonlinear optical crystal: L-tyrosine hydrobromide. Journal of Crystal Growth. 290 (2006) 498–503.

DOI : 10.1016/j.jcrysgro.2006.01.061

[24]. R.N. Jayaprakash and P. Kumaradass. Growth and Characterization of Urea L-Valine An Organic non Linear Optical Crystal. Orientation journal of chemistry. (2013), Vol. 29, No.4 : Page no. 1409-1414, ISSN: 0970-020 X.

[25]. Kuppan Venkatesan, Lakshmanan Jothi. Synthesis and Controllable Growth Dynamics of Third Order Nonlinear Optical Material of 2-Amino-4-Methylpyridinium 2-Chloro 4-Nitro Benzoate Electro-Mechanical Investigation and Device Fabrication. Journal of Minerals and Materials Characterization and Engineering. (2021), 9, 407-431.

DOI: 10.4236/jmmce.2021.95028

[26]. A. Anandhan , C. Sivasankari, M. Saravanabhavan , V. Siva , K. Senthil. Synthesis, crystal structure, spectroscopic investigations, physicochemical properties of third-order NLO single crystal for optical applications. (2019).

DOI : https://doi.org/10.1016/ j.molstruc.2019.127400.

[27]. A. Alexandar, P. Surendran, S. Sakthy Priya, A. Lakshmanan and P. Rameshkumar. Studies on growth and characterization of nonlinear optical L-tartaric acid–nicotinamide

single crystal. Journal of Nonlinear Optical Physics & Materials. Vol. 25, No. 3 (2016) 1650037 (19 pages).

DOI: 10.1142/S0218863516500375

[28]. R. Subhashini , S. Arjunan ,B. Gunasekaran. Synthesis of a metal coordinated amino acid based nonlinear single crystal, Bis (L-threonine) zinc (II) using the solution growth technique and its physicochemical properties. Journal of Physics and Chemistry of Solids 135 (2019) 109077.

DOI : https://doi.org/10.1016/j.jpcs.2019.109077

[29]. S. Sindhusha , C.M. Padma , B. Gunasekaran , H. Marshan Robert. Structural, optical and thermal analysis of creatininium borate e A new semiorganic nlo single crystal. Journal of Molecular Structure 1209 (2020) 127981.

DOI : https://doi.org/10.1016/j.molstruc.2020.127981

[30]. Mohd. Shakir, V. Ganesh, B. Riscob, K.K. Maurya, K. Kishan Rao, M.A. Wahab and G. Bhagavannarayana. Effect of L-Threonine Doping on Structural, Optical, Mechanical, Surface and Dielectric Properties of KDP Single Crystal. International Journal of Pure and Applied Physics ISSN 0973-1776 Volume 7, Number 1 (2011), pp. 13–24

[31]. N. Indumathi, A. Hemalatha, E. Chinnasamy, A. Venkatesan, M.E. Raja Saravanan, K. Deepa, P. Matheswar and, S. Senthil, K. Kaviyarasu, R. Uthrakumar. Synthesis and characterization of L-threonine lithium chloride (LTLC): A new semiorganic nonlinear optical single crystal for laser applications. Materials Today: Proceedings.

DOI : https://doi.org/10.1016/j.matpr.2020.02.669

[32]. Elberin Mary Theras, D. Anbuselvi, D. Jeyaraman, V. Joseph. Studies on growth and optical, structural, mechanical and photoconductivity of nonlinear optical material L-Threonine. International journal of chemTechResearch, July-Aug (2014), Vol. 6, No.4, pp: 2499-2506.

[33]. S. Ramalakshmi and K. A. Vijayalakshmi. Synthesis Growth and characterization studies of semi-organic NLO L-Valine calcium nitrate and L-Valine potassium nitrate single crystals. Rasayan J. Chem., 13(3), 1394-1400, (2020)

DOI : http://dx.doi.org/10.31788/RJC.2020.1335666

[34].S. E. Allen Moses, S. Tamilselvan, S. M. Ravi Kumar, G. Vinitha, Tejaswi Ashok Hegde, G. J. Shanmuga Sundar, M. Vimalan, S. Sivaraj. Crystal structure, spectroscopic, thermal, mechanical, linear optical, second order and third order nonlinear optical properties of semiorganic crystal: L-threoninium phosphate (LTP). Journal of Materials Science: Materials in Electronics. 24th April 2019

DOI : https://doi.org/10.1007/s10854-019-01229-9

[35]. P. Karuppasamy , T. Kamalesh , K. Anitha , S. Abdul Kalam , Muthu Senthil Pandian , P. Ramasamy , Sunil Verma , S. Venugopal Rao. Synthesis, crystal growth, structure and characterization of a novel third order nonlinear optical organic single crystal: 2-Amino 4,6-Dimethyl Pyrimidine 4-nitrophenol. Optical material 84, (2018), 475-489.

[36]. Rupali B. Kulkarnia. c, Mohd Anisb, S. S. Hussainid and Mahendra D. Shirsat. Transfiguring structural, optical and dielectric properties of Cadmium thiourea acetate crystal by the addition of L-threonine for laser assisted device applications. Journal of Materials Research Express.

DOI : https://doi.org/10.1088/2053-1591/aab2f8

[37]. V. M. Mahadevan, T. Thangeeswari and G. Parthipan. Thermal and nonlinear optical properties of semiorganic single crystal: L-Threonine p-nitrophenolate (LTPNP). IOP Conf. Series : Materials Science and Engineering. 764 (2020) 012012

DOI : 10.1088/1757-899X/764/1/012012

[38]. J. Elberin Mary Theras, D. Kalaivani, D. Jayaraman, V. Joseph. Growth and spectroscopic, thermodynamic and nonlinear optical studies of L-threonine phthalate crystal. Journal of Crystal Growth. (2015)

DOI : http://dx.doi. org/10.1016/j.jcrysgro.2015.06.009

[39]. R. Vivekanandhan, K. Raju, S. Sahaya Jude Dhas, V. Chithambaram. Investigation on Noval nonlinear Optical L-Threonine calcium chloride single crystal Grown by solution Growth Technique. International journal of applied Engineering Research, ISSN 0973-4562, Volume 13, Number 18, (2018), pp. 13454-13459.

[40]. Geetha Palani , Arul H , Sengottain Shanmugan and Chithambaram V. Growth, characterisation and antibacterial activity of LHCdBr single crystal, Materials Research Innovations, (2020).

DOI: 10.1080/14328917.2020.1814028

[41]. A.T. Ravichandran, R. Rathika, M. Kumaresavanji. Non-linear optical behaviour and antibacterial activity of semi-organic picolinic acid zinc sulphate single crystal. Materials Today: Proceedings 68 (2022) 502–505

DOI : https://doi.org/10.1016/j.matpr.2022.07.432

[42]. C. Muthuselvi, S. Manisha, R. S. Prabha. Growth, Spectral, Optical and Antibacterial Activity Studies on Glycine Hydrofluoride Single Crystal. International Journal of Research in Engineering and Science (IJRES). Volume 8 Issue 11 | 2020 | PP. 45-53

[43]. K. Balakrishnan, S. Sakthy Priya, A. Lakshmanan, P. Surendran, Karthik Kannan, P. Geetha, G. Vinitha, P. Praveen Kumar, P. Rameshkumar. Studies on structural, optical nonlinearity and antibacterial activity of Piperazine (bis) p-toluenesulfonate single crystal for optical limiting and biological applications. Physics and chemistry of solid state. Vol. 24, No. 1 (2023) pp. 46-55

DOI: 10.15330/pcss.24.1.46-55

[44]. Allen moses, S. Tamil selvan, S. M. Ravikumar, G. Vinitha, Tejaswi ashok hedge, M. Vimalan, S. varalakshmi, S. Sivaraj. Materials Science for Energy Technologies. 2, (2019), 565–574.

DOI : https://doi.org/10.1016/j.mset.2019.05.003

[45]. S. Amali Theresa, V. Shanthi, G.Rajesh Kanna, Aparna V.S, N.Mohan. Effect of L-threonine on the optical properties of (tris) thiourea zinc sulphate (TTZS) single crystal. International Journal of Aquatic Science. Vol 12, Issue 03, 2021. ISSN: 2008-8019.

[46]. A Shanthi, C Krishnan and P Selvarajan. Optical, mechanical and thermal characterization of l-threonine single crystals grown in dimethyl urea solution. Phys. Scr. 88, (2013), 035801.

DOI : 10.1088/0031-8949/88/03/035801

[47]. A. Puhal Raj, C. Ramachandra Raja. Synthesis, Growth, Structural, Spectroscopic, Thermal and Optical Properties of NLO Single Crystal: L-Threonine Zinc Acetate. Photonics and Optoelectronics (P&O) (www.jpo-journal.org). Volume 2 | Issue 3| July 2013.

[48]. A. Senthilkumar, K. Sambathkumar, S. Nithiyanantham, M. Venkatachalapathy, N. Rajkamal, Structural, chemical and physical Properties of pure and La3+ doped l-Threonine Acetate Crystals, Journal of Molecular Structure, (2017).

DOI : 10.1016/j.molstruc. 2017.08.012.

[49]. S. Manivannan, S. Dhanuskodi. Synthesis, crystal growth, structural andoptical properties of an organic NLO material. Journal of Crystal Growth. 262, (2004), 473–478.

DOI : 10.1016/j.jcrysgro.2003.10.029

[50]. C. Ramachandra Raja, A. Antony Joseph. Crystal growth and comparative studies of XRD, spectral studies on new NLO crystals: l-Valine and l-valinium succinate. Spectrochimica Acta Part A 74, (2009), 825–828.

DOI : 10.1016/j.saa.2009.08.023

[51]. B. Sahaya Infant Lasalle , Muthu Senthil Pandian , K. Anitha , P. Ramasamy. Single crystal growth of 1,2,3-Benzotriazole 3,5-dinitrobenzoic acid (BTNBA) by slow evaporation solution technique (SEST) for nonlinear optical (NLO) applications. Inorganic chemistry communications. 162, (2024), 112190.

DOI : https://doi.org/10.1016/j.inoche.2024.112190

[52]. Suresh Sagadevan and Priya Murugasen. Growth, Microhardness, Electrical and Dielectric Studies on L-Alanine Hydrogen Chloride NLO Single Crystal. International Journal of Materials Science and Engineering. Volume 3, Number 2, June 2015.

DOI : 10.17706/ijmse.2015.3.2.159-166

[53]. V. Vasantha Kumari , P. Selvarajan and R. Thilagavathi. Growth and characterization of L-proline potassium bromide: A semiorganic NLO crystal. Journal of Chemical and Pharmaceutical Research, 2015, 7(9):133-143.

[54]. Fredselin R.S Vithel, R. Manimekalai. Growth and characterization of L-phenyl alanine added sulphamic acid single crystals. Journal of Advanced Scientific Research. (2021), 12 (2) Suppl 1, 145-152. ISSN : 0976-9595.

[55]. N. Rajasekar, K. Balasubramanian. Crystallization and multifaceted characterization of L-Asparagine monohydrate single crystals for structural, spectroscopic, Optical, Thermal and morphological analysis toward for Third order NLO applications. International Journal of Applied Mathematics. Volume 38, No. 10s, (2025). ISSN: 1311-1728 (printed version); ISSN: 1314-8060 (on-line version)

DOI : https://doi.org./10.12732/ijam.v38i10s.992